NIH Public Access
Author Manuscript
Cancer Res. Author manuscript; available in PMC 2013 September 01.

Published in final edited form as:
Cancer Res. 2012 September 1; 72(17): 4483–4493. doi:10.1158/0008-5472.CAN-12-0283.

Dual targeting of the Akt/mTOR signaling pathway inhibits castration-resistant prostate cancer in a genetically engineered mouse model

Nicolas Floc'h[1,4], **Carolyn Waugh Kinkade**[1,4], **Takashi Kobayashi**[1,4], **Alvaro Aytes**[1,4], **Celine Lefebvre**[2,4], **Antonina Mitrofanova**[2,4], **Robert D. Cardiff**[5], **Andrea Califano**[2,4], **Michael M. Shen**[3,4], and **Cory Abate-Shen**[1,4]

[1]Departments of Urology and Pathology and Cell Biology, Columbia University Medical Center, New York, NY 10032

[2]Department of Biomedical Informatics and Center for Computational Biology and Bioinformatics, Columbia University Medical Center, New York, NY 10032

[3]Departments of Medicine and Genetics & Development, Columbia University Medical Center, New York, NY 10032

[4]Herbert Irving Comprehensive Cancer Center, Columbia University Medical Center, New York, NY 10032

[5]Center for Comparative Medicine and Department of Pathology, School of Medicine, University of California, Davis 95616

Abstract

While the prognosis for clinically localized prostate cancer is now favorable, there are still no curative treatments for castration-resistant prostate cancer and, therefore, remains fatal. In this study, we investigate a new therapeutic approach for treatment of castration-resistant prostate cancer, which involves dual targeting of a major signaling pathway that is frequently deregulated in the disease. We found that dual targeting of the Akt and mTOR signaling pathways with their respective inhibitors, MK-2206 and ridaforolimus (MK-8669), is highly effective for inhibiting castration-resistant prostate cancer in preclinical studies *in vivo* using a refined genetically-engineered mouse model of the disease. The efficacy of the combination treatment contrasts with their limited efficacy as single agents, since delivery of MK-2206 or MK-8669 individually had a modest impact *in vivo* on the overall tumor phenotype. In human prostate cancer cell lines, although not in the mouse model, the synergistic actions of MK-2206 and ridaforolimus (MK-8669) are due in part to limiting the mTORC2-feedback activation of Akt. Moreover, the effects of these drugs are mediated by inhibition of cellular proliferation via the retinoblastoma (RB) pathway. Our findings suggest that dual targeting the Akt and mTOR signaling pathways using MK-2206 and ridaforolimus (MK-8669) may be effective for treatment of castration-resistant prostate cancer, particularly for patients with deregulated RB pathway activity.

Keywords

Akt/mTOR signaling; castration-resistant prostate cancer; genetically engineered mouse models; preclinical analyses; *Pten*; *RB*

Author for correspondence: Cory Abate-Shen Columbia University Medical Center 1130 St. Nicholas Ave. New York, NY 10031 Phone: (212) 851-4735 Fax: (212) 851-4787 cabateshen@columbia.edu.

Disclosure: This work was supported in part by funding from Merck.

NIH-PA Author Manuscript
NIH-PA Author Manuscript
NIH-PA Author Manuscript

NIH-PA Author Manuscript

NIH-PA Author Manuscript

NIH-PA Author Manuscript

Introduction

All aspects of prostate development and function require androgen signaling, which is mediated by the androgen receptor (AR), a nuclear steroid receptor (1, 2). Moreover, prostate cancer arises under the influence of AR signaling, while removal of androgens via androgen deprivation therapy is the most common first-line treatment for recurrent prostate tumors. However, in most cases androgen deprivation therapy ultimately results in the emergence of a highly aggressive form of the disease, which is now referred to as "castration-resistant prostate cancer" (CRPC) to reflect its continued dependence on AR in the absence of testicular androgens (3). Among available therapeutic approaches for treatment of CRPC, conventional chemotherapy has limited efficacy (4-6). Recently, several agents that target AR and/or androgen synthesis, namely MDV3100 and Abiraterone, have been introduced into the clinic and have shown with promising results (7, 8), although they are also not curative.

An alternative approach is targeted therapy directed against signaling pathways that are active in CRPC, including the Akt/mTOR signaling axis. Indeed, the culmination of several lines of evidence, including analyses of tissue microarrays (9-11), oncogenomic analyses of human clinical data (12), and functional studies in mouse and human prostate cancer cells (9, 13, 14), have established that activation of Akt/mTOR signaling is strongly and causally associated with advanced prostate tumors and particularly CRPC. Nonetheless, despite the relevance of Akt/mTOR pathway deregulation for disease progression and the availability of suitable therapeutic agents, targeting these pathways using single agents has not been effective in clinical settings (15, 16), although there are notable exceptions (17). It is widely believed that this may be due in part to feedback activation of these pathways, which occurs in response to drug treatment (18-21).

Therefore, we have now investigated the consequences of dual targeting Akt/mTOR signaling in CRPC. By analyses of preclinical studies *in vivo* using genetically-engineered mouse models (GEM models), we show that combinatorial treatment using MK-2206 to target Akt and ridaforolimus (MK-8669) to target mTOR is highly effective for inhibition of CRPC. Parallel studies of human prostate cancer cell lines in culture revealed that the mechanism of action is via inhibition of cellular proliferation mediated by the retinoblastoma (RB) signaling pathway. Considering the importance of RB status for progression to CRPC (12, 22) as well as response to therapy (23), our findings suggest that dual inhibition of Akt/mTOR signaling with MK-2206 and MK-8669 may be a promising approach for treatment of patients with CRPC, particularly those with deregulated RB signaling.

Materials and Methods

Generation and analysis of GEM models

All experiments using animals were performed according to protocols approved by the Institutional Animal Care and Use Committee at Columbia University Medical Center. The *Nkx3.1*$^{CreERT2/+}$ allele, which is null for *Nkx3.1*, expresses Cre-ERT2 under the control of the *Nkx3.1* promoter (24). The conditional allele for *Pten* (*Pten*$^{flox/flox}$) having loxP sites flanking exon 5 (25) was obtained from the NCI Mouse Models of Human Cancer Consortium. Mice were breed to generate the full spectrum of genotypic combinations. Primers for genotyping are provided in Supplementary Table 1.

For induction of Cre activity, Tamoxifen (Sigma Cat #T5648) (or corn oil alone) was delivered by IP injection (225mg/kg) or oral gavage (100 mg/kg) for 4 consecutive days, to

NIH-PA Author Manuscript

NIH-PA Author Manuscript

NIH-PA Author Manuscript

mice at 2-3 months of age. Mice were androgen-ablated by surgical castration at 4 months. For phenotypic analyses, mice were sacrificed, the prostatic lobes (anterior, dorsolateral, and ventral) were collected individually and the weights determined. Tissues were fixed in 10% formalin, cyropreserved in Optimal Cutting Temperature (OCT) compound, or snap-frozen in liquid nitrogen.

Immunohistochemical staining was done on 3 μm paraffin sections as described previously (9) using an Intellipath FLX from Biocare Medical (Concord, CA) and visualized using a Nikon Eclipse E800 microscope equipped with a Nikon DXM1200 digital camera. Quantification of proliferating cells was done as described previously (26), using 5 independent sections from 5 independent mice (*i.e.*, 25 sections). SA β-galactaside staining was done on tissues embedded directly in OCT (without prior fixation) as in (27). Western blot analyses were done using total protein extracts obtained by sonicating mouse prostate tissue or human prostate cell in 1X RIPA buffer (0.1% SDS, 1.0% Deoxycolate-Sodium Salt, 1.0% Triton X-100, 0.15 M NaCl, 10 mM Tris-HCl (pH 7.5), 1 mM EDTA) containing fresh 1% protease inhibitor (Roche Basel, Switzerland #1697498) and 1% phosphatase inhibitor (Sigma-Aldrich St. Louis, Missouri #P2850). Details of all antibodies are provided in Supplementary Table 2.

Real-time PCR was done on total RNA using the Quantitech SYBR Green PCR kit (Qiagen). A Pair Wise Fixed Reallocation Randomization Test using the Relative Expression Software Tool (REST) (Qiagen) was used to test the significance of the expression ratios of transcripts. Primers are listed in Supplementary Table 1. Statistical analyses were performed using a two-tailed T-test, X^2 test, or Fisher's Exact test as appropriate. GraphPad Prism software (Version 5.0) was used for all statistical analysis and to generate data plots.

Preclinical analyses of genetically-engineered mice

MK-2206 and MK-8669 were obtained from Merck. MK-2206 was dissolved in 30% captisol (Cydex) in sterile water to make a working stock of 20mg/mL and delivered via oral gavage at 120 mg/kg. MK-8669 was dissolved in 100% ethanol to make a working stock of 25 mg/ml, and then diluted to 1.25 mg/ml in a solution of 5.2% Tween 80, 5.2% PEG400 in sterile water and delivered via IP at 10 mg/kg. Docetaxel was purchased from LC Labs and delivered at 10 mg/kg in a vehicle solution of 23% Tween 80 in 1 X PBS. The optimal dosage of each of drug was determined by delivering varied amount of drug over a period of one month to mice of the same strain and genotypic background used for the preclinical studies, and selecting the maximal tolerated dose. The starting point for these dosage studies was the information provided by the supplier (Merck). The MK-2206 and/or MK-8669 (or vehicle) were delivered three times a week (Monday, Wednesday, and Friday) and docetaxel was delivered twice a week (Tuesday, Friday) for a period of two months. For the short-term therapeutic response group, agents were delivered once a day for 5 consecutive days, and mice were dissected 6 hours after last treatment. Mice were weighed daily and observed for signs of distress following dosing; none of the treatments resulted in appreciable weight loss exceeding 10%.

Computational analyses of expression profiling data

Gene expression profiling analysis was done using total RNA isolated form phenotypically wild-type (intact) *Nkx3.1*$^{CE2/+}$ (n = 3), intact *Nkx3.1*$^{CE2/+}$; *Pten*$^{f/f}$ (n = 6), and castrated *Nkx3.1*$^{CE2/+}$; *Pten*$^{f/f}$ (n = 6). RNA was isolated using the MagMAX-96 total RNA isolation kit (Ambion), which was reverse-transcribed and biotin-labeled using the Illumina TotalPrep RNA Amplification kit (Ambion). The cRNA (1.5 mg) was hybridized on mouseWG-6 v2 BeadArrays (Illumina) using an iScan BeadArray scanner (Illumina). Data were imported

NIH-PA Author Manuscript

NIH-PA Author Manuscript

NIH-PA Author Manuscript

and corrected for background using Illumina BeadStudio 3.2 package and normalized using the R-system v2.11.1 lumi library. Data were normalized using IlluminaExpressionFileCreator version 2 with collapse mode using the maximum of all the probe values for each gene and without background subtraction. The resulting datasets were preprocessed to remove probesets whose minimum fold change (maximum gene expression value divided by the minimum value) was <3, or whose difference between maximum and minimum values were less than 100.

Gene signatures comparing the intact wild-type (*Nkx3.1*$^{CE2/+}$) to the intact and castrated *Nkx3.1*$^{CE2/+}$; *Pten*$^{f/f}$ were defined using the Welch T-test to identify genes ranked by their differential expression in the intact and castrated *Nkx3.1*$^{CE2/+}$; *Pten*$^{f/f}$ mouse prostate tumors versus the phenotypically-wild-type (*Nkx3.1*$^{CE2/+}$) mouse prostate, respectively. To identify pathways commonly deregulated in intact and castrated *Nkx3.1*$^{CE2/+}$; *Pten*$^{f/f}$ prostate tumors, enrichment of these differentially expressed gene signatures in human pathways was evaluated using GSEA (28) using pathways collected in the c2 curated gene sets (http://www.broadinstitute.org/gsea/msigdb/index.jsp) with 1,000 gene label permutations (gene-sets). Significantly enriched gene sets, defined by nominal p-value <0.05, were compared between intact "*Nkx3.1*$^{CE2/+}$; *Pten*$^{f/f}$ versus *Nkx3.1*$^{CE2/+}$" and castrated intact "*Nkx3.1*$^{CE2/+}$; *Pten*$^{f/f}$ versus *Nkx3.1*$^{CE2/+}$" gene signatures. Enrichment analyses to identify relevant biological processes were done by interrogating the REACTOME (29), KEGG (30), and BioCarta (http://www.biocarta.com/genes/allpathways.asp) databases.

Cell culture analyses

PC3 (CRL-1435™) and LNCaP (CRL-1740™) cells were obtained from the American Type Culture Collection (ATCC; Bethesda, MD, USA) and were used within 6 months of their receipt; verification of the cell lines was done by ATCC. Cells were grown in a RPMI medium supplemented with 10% heat-inactivated fetal calf serum (FCS) and 100 U/ml penicillin–streptomycin. Cells were treated with Vehicle (DMSO) or with MK-2206 (1 μM) and/or MK-8669 (1 nM) for 24-96 hours (as indicated). Where indicated, 12.5 nM siRNA or control siRNA (Ambion, Austin, TX) were introduced by transfection using Lipofectamine™ RNAiMAX (Invitrogen, Carlsbad, CA). All cell culture assays were done in at least three independent experiments. Comparison of differences among the groups was carried out by two-tailed Student's *t*-test.

Results

A refined mouse model of castration-resistant prostate cancer

Among the genes that are known to be causally associated with prostate tumorigenesis are: *(i)* the *Nkx3.1* homeobox gene, which is specifically expressed in the prostatic epithelium and its reduced expression associated with prostatic intraepithelial neoplasia (PIN) (1, 31); and *(ii)* the *Pten* tumor suppressor, whose loss of function is associated with tumor promotion via activation of the PI3K/Akt signaling pathway (1, 32, 33). Previously we showed that germline loss-of-function of *Pten* and *Nkx3.1* leads to CRPC following surgical castration (34, 35), and other groups have shown that conditional loss-of-function of *Pten* in prostate also leads to CRPC (36-39). Indeed, several lines of evidence now support a causal role for *Pten* loss of function in the transition to CRPC (13, 39, 40), and therefore highlight the importance of using GEM mice based on *Pten* inactivation to study CRPC *in vivo*. However, germline loss of *Pten* results in tumors in many sites other than prostate, while most of the conditional deletion models reported thus far have used a constitutively-active Probasin-Cre transgene (*PB-Cre4*), which leads to recombination (deletion) in the prostate prior to complete maturation (41).

NIH-PA Author Manuscript

NIH-PA Author Manuscript

NIH-PA Author Manuscript

In the current study, we produced a refined GEM model of *Pten*-induced castration resistance by deleting *Pten* specifically in the prostatic epithelium of adult mice using a tamoxifen-inducible (rather than constitutively active) Cre under the control of the *Nkx3.1* promoter (24). This $Nkx3.1^{CreERT2}$ knock-in allele simultaneously inactivates one allele of *Nkx3.1* (which is haploinsufficient in prostate cancer (1, 31)) while driving tamoxifen-dependent Cre-mediated recombination specifically in prostate epithelium, including in a relevant cell of origin of prostate cancer (24). This $Nkx3.1^{CreERT2}$ allele was crossed with a *Pten* conditional allele (25) to obtain the $Nkx3.1^{CreERT2/+}; Pten^{flox/flox}$ mice used in these studies (hereafter denoted $Nkx3.1^{CE2/+}; Pten^{f/f}$). Importantly, *Pten* recombination was induced via tamoxifen-activation of Cre in adult mice at 2 months of age, which is subsequent to when the prostate and other male secondary sexual organs are fully mature. In control experiments, we have demonstrated that this temporally-limited induction with tamoxifen has little or no effect on the prostate phenotype of control or mutant mice (24).

The $Nkx3.1^{CE2/+}; Pten^{f/f}$ mice, but not the control mice ($Nkx3.1^{CE2/+}$), developed PIN lesions as early as 6-7 months after tamoxifen induction, which by 9 to 12 months progressed to high-grade PIN (N = 8/8 mice) and by 16 months to extensive high-grade PIN with areas of invasion (N = 8/8 mice; Figure 1A-E; Table 1). Pathological evaluation of these lesions using the classification of Park et al. (42) revealed that mouse tumors displayed extensive PIN III and PIN IV (i.e., high grade PIN) with areas of squamous metaplasia, found in some GEM models of prostate cancer.

$Nkx3.1^{CE2/+}; Pten^{f/f}$ mice that have undergone depletion of androgens by surgical castration initially display tumor regression (N= 4/4 mice), which is evident by 2 weeks following castration (Figure 1I-L). However, this initial regression was followed by the emergence of castration-resistant lesions that resembled high-grade PIN by 6-7 months after tamoxifen induction (N = 14/14 mice); these lesions progressed to high-grade PIN with adenocarcinoma by 12 months and to extensive, poorly differentiated adenocarcinoma by 16 months following tamoxifen induction (N = 14/14 mice; Figure 1F-H; Table 1). Pathological evaluation of these lesions (42) revealed that these tumors displayed extensive PIN IV (N = 14/14 mice) and some with squamous metaplasia (N = 2/14 mice) by 12 months following tumor induction, while the older mice (i.e., 16 months) displayed extensive microinvasive adenocarcinoma, which was not evident in the non-castrated mice (N = 14/14 mice; Table 1). Therefore, the $Nkx3.1^{CE2/+}; Pten^{f/f}$ mice are initially sensitive to castration as has been reported previously for *Pten* inactivation in other GEM models (34, 36), but ultimately develop castration-resistant tumors that are histologically more advanced than the intact mice.

Notably, although the castrated $Nkx3.1^{CE2/+}; Pten^{f/f}$ mice had a more severe phenotype, immunochemical analyses revealed that the lesions arising in prostates from the intact and castrated mice were otherwise more similar than they were different (Figure 2). In particular, the prostatic lesions in both the intact and castrated mice expressed robust levels of AR, which was mainly nuclear (n = 5; Figure 2A,B). These prostatic lesions were primarily epithelial, as evident from the robust expression of cytokeratin 8 (CK8), a marker of luminal epithelium, although the prostatic lesions from the castrated mice displayed an ~5 fold increase in the basal cells, evident from expression of cytokeratin 5 (CK5), a basal cell marker (n = 5; Figure 2C-F, Q). Furthermore, both the intact and castrated prostates were similarly highly proliferative (~12-14%) as evident by Ki67 staining (n = 5; Figure 2G,H; Table 1). Finally, the prostatic lesions in both the intact and castrated mice displayed strong activation of Akt and mTOR signaling, as evident by the immunostaining for p-Akt and p-S6, respectively, as well as by Western blot analyses (Figure 2I-L, Q).

NIH-PA Author Manuscript

NIH-PA Author Manuscript

NIH-PA Author Manuscript

Nonetheless, lesions arising in prostates of castrated *Nkx3.1*$^{CE2/+}$; *Pten*$^{f/f}$ mice were consistently more advanced than those of the age-matched intact *Nkx3.1*$^{CE2/+}$; *Pten*$^{f/f}$ mice (Figure 1; Table 1). Interestingly, this was accompanied by decreased expression of senescence-associated (SA) β-galactosidase. In particular, while prostates from the intact *Nkx3.1*$^{CE2/+}$; *Pten*$^{f/f}$ mice expressed high levels of SA-β-galactosidase (SA-β-gal), as has been reported previously for other prostate cancer models based on inactivation of *Pten* (27), SA-β-gal expression was barely detectable in prostates from the castrated *Nkx3.1*$^{CE2/+}$; *Pten*$^{f/f}$ prostate (Figure 2M-P). Notably, this striking difference in SA-β-gal expression was observed in mice at 7 months following tumor induction (3 months after castration) (Figure 2M,N), when both the intact and castrated mice display a similar histopathology (see Figure 1, Table 1), indicating that this difference is not due to the more advanced nature of the castrated tumors. These findings raise the interesting possibility that castration-resistance is associated with a bypass of the senescence phenotype, which may contribute to cancer progression.

Computational analyses using gene expression profiling (Supp. Table 3, 4) supports our observations from these phenotypic analyses that the prostate tumors from intact and castrated *Nkx3.1*$^{CE2/+}$; *Pten*$^{f/f}$ mice are more similar than they are different. In particular, using gene set enrichment analyses (GSEA) (28) to identify relevant biological processes, we found that about 50% of biological pathways were similarly deregulated in prostates of both intact and castrated mice (Figure 2R; Supp. Tables 6, 7). Among the pathways that were similarly deregulated between the intact and castrated *Nkx3.1*$^{CE2/+}$; *Pten*$^{f/f}$ prostate tumors were the *NFκB* signaling, which is an indicator of the relative levels of inflammation, and the p53 pathway, which has been associated with abrogating the senescence phenotype following *Pten* inactivation (27) (Supp. Tables 6, 7). Therefore, both the phenotypic and molecular features of the intact and castrated *Nkx3.1*$^{CE2/+}$; *Pten*$^{f/f}$ mouse prostate tumors support the fact that they are highly similar.

Interestingly, the notable exception to this overall similarity was deregulation of a senescence signature ($p < 0.001$), which was only observed in the intact prostate (Figure 2S), consistent with our phenotypic observation (Figure 2M-P). Taken together, these findings further support a critical role for *Pten* loss-of-function for castration-resistance and suggest that the transition to castration-resistance is associated with alleviation of the senescence phenotype, which may contribute to the more aggressive phenotype of castrate-resistant tumors.

Combination targeted therapy inhibits castration-resistant prostate cancer

Although in general, targeted therapy using single agents directed against Akt/mTOR signaling has had limited efficacy in clinical contexts (15, 16), their actions as combined agents has shown some promise, including in prostate cancer cells (43). Given the robust activation of Akt and mTOR signaling in these mouse tumors (see Figure 2I-L), we considered that the castrated *Nkx3.1*$^{CE2/+}$; *Pten*$^{f/f}$ mice are well suited to evaluate the consequences of combinatorial targeting these signaling pathways for inhibition of CRPC. To do so, we used a specific non ATP-competitive allosteric Akt inhibitor, MK-2206, that is highly effective for inhibiting Akt function in various *in vivo* and cellular contexts (17, 44, 45). We combined this Akt inhibitor with an mTOR inhibitor, MK-8669 (ridaforolimus, formerly termed deforolimus), an analog of rapamycin specific for the mTORC1 complex (11). Both of these agents have been evaluated in clinical trials where they have been shown to be effective and well-tolerated (17, 46-48), and the combination is currently being tested in a Phase I trial (clinicaltrials.gov #NCT01295632). Notably, we verified that each of these agents inhibited their respective pathways in the mouse prostate *in vivo* when delivered individually or in combination (Figure 3G-P, V), and were well-tolerated for the duration of the treatment period when delivered at their effective doses.

NIH-PA Author Manuscript

NIH-PA Author Manuscript

NIH-PA Author Manuscript

Thus, we performed preclinical studies in the intact or castrated *Nkx3.1*$^{CE2/+}$*; Pten*$^{f/f}$ mice by administering MK-2206 and/or MK-8669 for 2 months, following which the mice were sacrificed for analysis (Figure 3A; Supp. Figure 1 and Supp Table 3). Treatment with either MK-2206 or MK-8669 alone had a modest impact on the overall tumor phenotype considering multiple endpoints (see below), although MK-8669 significantly reduced proliferation (Table 2). In striking contrast, the combination of MK-2206 + MK-8669 was highly effective for inhibiting castration-resistant tumors (Figure 3 and Table 2). This was evident by analyses of several independent endpoints, including: *(i)* a profound alteration in histological phenotype (Figure 3B-F); *(ii)* a 13-fold reduction in tumor weight ($p = 0.004$) (Table 2); *(iii)* a significant (3-fold) reduction in cellular proliferation ($p < 0.001$) (Figure 3Q-U, Table 2); and *(iv)* attenuated expression of the relevant pathway markers, namely p-Akt and p-S6 (Figure 3G-P, V). Notably, MK-2206 + MK-8669 had only a modest effect on the tumor phenotype in the intact *Nkx3.1*$^{CE2/+}$*; Pten*$^{f/f}$ mice as evident by the more limited effect on tumor weight, histology and other end points, although these agents were still more effective in combination than individually (Supp. Figure 1, Supp. Table 3). Interestingly, the strong efficacy of MK-2206 + MK-8669 for inhibition of these castration-resistant tumors contrasted with the weak efficacy of conventional chemotherapy (Docetaxel) (Figure 3F, K, P, U, W), paralleling the limited efficacy of conventional chemotherapy for CRPC in humans (6). Taken together, these preclinical studies suggest that dual targeting Akt/mTOR signaling using MK-2206 + MK-8669 may be beneficial for treatment of CRPC.

Dual targeted therapy Akt/mTOR signaling affects RB signaling

We next sought to understand the mechanism of action of MK-2206 + MK-8669 in human prostate cancer cells in culture, using PC3 and LNCaP cells (49) (Figure 4). First, we confirmed that these drugs inhibit their respective signaling pathways by assessing phosphorylation at serine 473 on Akt to evaluate inhibition by MK-2206, and phosphorylation of S6 and 4E-BP1, which are specific for mTORC1, as a read-out of MK-8669 activity. As expected, the Akt (MK-2206) and mTOR (MK-8669) inhibitors each restrain their respective pathways in these human prostate cancer cells, as evident by Western blot analyses (Figure 4A). However, in both cell lines, treatment with the mTOR inhibitor resulted in up-regulation of Akt phosphorylation specifically at serine 473 (Figure 4A). Interestingly, this was not observed in the mouse model (see Figure 3), reflecting a difference in the mouse model and human cancer cell lines.

It has been reported that in human cancer cells, mTORC1 inhibition can result in phosphorylation of Akt at serine 473 as a consequence of mTORC2 complex activation in a Rictor-dependent manner (18). Indeed, we found that siRNA knock-down of Rictor effectively abrogated the MK-8669-dependent up-regulation of p-Akt at serine 473 (Figure 4B). These observations suggest that the enhanced efficacy of MK-2206 + MK-8669, at least in human cells, may be due in part from overcoming the consequences of feedback activation that occurs when targeting the Akt/mTOR pathway with single agents.

Next we examined the functional consequences of treatment with MK-2206 + MK-8669 on the human prostate cancer cell lines. While these agents used individually or in combination had no apparent effect on apoptosis or autophagy (data not shown), they had a significant effect on cellular proliferation, as shown in PC3 cells (Figure 4D) but also seen in LNCaP cells (data not shown). In particular, treatment with either MK-2206 or MK-8669 individually resulted in a 1.8- or 2.0-fold reduction in cellular proliferation, respectively, while combined treatment with MK-2206 + MK-8669 resulted in a 2.6-fold reduction ($p < 0.0001$). This was accompanied by an increase in the percentage of cells in G_1, from 41% for the vehicle-treated cells to 53 or 55% in the cells treated with each agent individually, and 75% in the cells treated with both agents together ($p < 0.0001$; Figure 4E). It is noteworthy that the combined action of MK-2206 + MK-8669 is additive in cell culture, in

NIH-PA Author Manuscript

NIH-PA Author Manuscript

NIH-PA Author Manuscript

contrast to their synergistic effects *in vivo* (compare Figures 3 and 4), as observed previously with another combination targeted therapy (9, 14). This may reflect additional non-cell autonomous consequences of these agents *in vivo*, such as effects on angiogenesis or other processes (50) and/or the duration of the treatment period, which is 2 months *in vivo* but only a few days *in vitro*.

Finally, we considered the mechanisms by which MK-2206 + MK-8669 inhibited cellular proliferation using Western blot analyses to assess the status of potential effectors. We found that treatment with both MK-2206 + MK-8669, but not either agent individually, resulted in a significant reduction in RB phosphorylation at two key serines [Ser(807/811) and Ser(780)] (Figure 4C) which are targets of Cyclin E/CDK2 and Cyclin D/CDK4, respectively. Considering that a major target of the RB protein is the S-phase-inducing transcription factor E2F1 (51), we evaluated the status of E2F target genes in the castrated *Nkx3.1*$^{CE2/+}$*; Pten*$^{f/f}$ prostate tumors (Figure 5). Using GSEA pathway analyses, we observed a significant activation of the E2F signaling pathway in the castration-resistant tumors (Figure 5A, B). Furthermore, real-time qPCR validation of relevant target genes revealed that E2F target genes that were up-regulated in the *Nkx3.1*$^{CE2/+}$*; Pten*$^{f/f}$ prostate tumors, relative to the control prostate (*i.e., Nkx3.1*$^{CE2/+}$) were accordingly down-regulated following treatment with MK-2206 + MK-8669 (*e.g., XDH, PLAT, TAGLN2, and CD74*; Figure 5C). Taken together, these findings suggest that the observed inhibition of CRPC by dual targeting the Akt/mTOR signaling pathway with MK-2206 + MK-8669 is mediated by negative regulation of cellular proliferation through the RB signaling pathway. Considering that the RB pathway is one of the key pathways affected in CRPC (12, 22), drugs that affect RB pathway activity may be advantageous for a significant number of patients.

Discussion

In this study, we provide *in vivo* preclinical evidence from a refined GEM model of castration-resistant prostate cancer (CRPC), complemented by analyses of human prostate cancer cells in culture, to demonstrate the efficacy of dual targeting of Akt/mTOR signaling for treatment of CRPC. An important feature of our refined GEM model is that tumors arise following inducible *Pten* inactivation in the adult prostate, which differs from previous GEM models based on conditional inactivation of *Pten* in immature prostate epithelium, or its germline loss of function (34, 36, 38). Nonetheless, in this new GEM model, as was the case for the previous ones (34, 36), castration results in an initial regression, followed the emergence of castration-resistant tumors that are more aggressive than their non-castrated counterparts. Importantly, our findings indicate that these castration-resistant tumors, which are otherwise quite similar to their non-castrated counterparts, display a virtual absence of senescence, which is a hallmark of *Pten* loss-driven prostate tumors (27). Thus, our findings support the idea that cellular senescence restrains *Pten* loss-driven prostate tumors (27), and further suggests that castration unleashes a more aggressive form of the disease by bypassing senescence.

Our preclinical findings in this GEM model and complementary studies using human prostate cancer cells, along with a previous cell culture study (43), suggest that the combined use of agents targeting distinct components of Akt/mTOR signaling may be advantageous, in part because they overcome a feedback loop that is believed to limit the efficacy of single agents. However, it is important to note that the observed consequences of these agents may differ when evaluated in cell culture versus *in vivo* and in human cells versus mouse models (52). In particular, while a feedback mechanism was readily evident in our analyses of human prostate cancer cell lines in culture (see Figure 4), we did not observe this in our analyses of the GEM mice *in vivo* (see Figure 3). Other studies have shown that although rapamycin blocks S6 phosphorylation, but not Akt^{S473} phosphorylation in various

NIH-PA Author Manuscript

NIH-PA Author Manuscript

NIH-PA Author Manuscript

cell lines, prolonged exposure to rapamycin can also target mTORC2 (53). Therefore, additional factors *in vivo* may contribute to the enhanced efficacy of the dual inhibition Akt/mTOR signaling, in addition to limiting feedback inhibition. Furthermore, our findings indicate that dual inhibition of Akt/mTOR signaling with MK-2206 + MK-8669 is linked to inhibition of cellular proliferation via the RB signaling pathway, which is deregulated in a large subset of patients with CRPC (12, 22).

Based on our findings showing the enhanced efficacy of dual inhibition of Akt/mTOR signaling, we propose that the combination of MK-2206 + MK-8669 should be evaluated in clinical trials for patients with CRPC. Given the intractable nature of this disease, which has resisted many treatment modalities thus far, we further suggest that MK-2206 + MK-8669 should be considered as part of a broader treatment regime that includes agents directed toward alternative mechanisms relevant for the disease. In this regard, the AR agonist, MDV3100, has shown tremendous promise in the clinic (8), has improved efficacy in combination with a PI3 kinase inhibitor in castration-resistant GEM mice (36). Therefore, it will be of interest to evaluate MK-2206 + MK-8669 combined with agents that target androgen signaling, such as MDV3100 as well as Abiraterone. Additionally, our intriguing finding showing the inverse correlation of castration-resistance and cellular senescence suggests the possibility of combining MK-2206 + MK-8669 with a pro-senescence therapy, as proposed by Pandolfi and colleagues (54). Such combinations can be readily evaluated in preclinical studies using these GEM mice, which can provide an initial assessment of the efficacy of the various combinations, as well as mechanistic insights into drug actions. In summary, we propose that dual targeting of Akt/mTOR signaling using MK-2206 + MK-8669 may contribute to a treatment regime for CRPC.

Supplementary Material

Refer to Web version on PubMed Central for supplementary material.

Acknowledgments

This work was supported by grants CA084294 (to CAS, MMS and AC), CA154293 (to MMS and CAS), U54CA121852 (to AC) and an award from the V-Foundation for Cancer Research to CAS. AA is a recipient of a Marie Curie International Outgoing Fellowship (PIOF-GA-2009-253290), co-sponsored with the Catalan Institute of Oncology-Bellvitge Institute for Biomedical Research, Barcelona, Spain. TK was supported by post-doctoral training grants from the American Urological Association Foundation and the American Association for Cancer Research. AM is a recipient of a National Science Foundation Post-doctoral Training Grant (#0937060). CAS is an American Cancer Society Research Professor supported in part by a generous gift from the F.M. Kirby Foundation.

References

1. Shen MM, Abate-Shen C. Molecular genetics of prostate cancer: new prospects for old challenges. Genes Dev. 2010; 24:1967–2000. [PubMed: 20844012]
2. Gelmann EP. Molecular biology of the androgen receptor. J Clin Oncol. 2002; 20:3001–15. [PubMed: 12089231]
3. Scher HI, Sawyers CL. Biology of progressive, castration-resistant prostate cancer: directed therapies targeting the androgen-receptor signaling axis. J Clin Oncol. 2005; 23:8253–61. [PubMed: 16278481]
4. Petrylak DP, Tangen CM, Hussain MH, Lara PN Jr. Jones JA, Taplin ME, et al. Docetaxel and estramustine compared with mitoxantrone and prednisone for advanced refractory prostate cancer. N Engl J Med. 2004; 351:1513–20. [PubMed: 15470214]
5. Tannock IF, de Wit R, Berry WR, Horti J, Pluzanska A, Chi KN, et al. Docetaxel plus prednisone or mitoxantrone plus prednisone for advanced prostate cancer. N Engl J Med. 2004; 351:1502–12. [PubMed: 15470213]

NIH-PA Author Manuscript

NIH-PA Author Manuscript

NIH-PA Author Manuscript

6. Pienta KJ, Smith DC. Advances in prostate cancer chemotherapy: a new era begins. CA Cancer J Clin. 2005; 55:300–18. quiz 23-5. [PubMed: 16166075]
7. de Bono JS, Logothetis CJ, Molina A, Fizazi K, North S, Chu L, et al. Abiraterone and increased survival in metastatic prostate cancer. N Engl J Med. 2011; 364:1995–2005. [PubMed: 21612468]
8. Scher HI, Beer TM, Higano CS, Anand A, Taplin ME, Efstathiou E, et al. Antitumour activity of MDV3100 in castration-resistant prostate cancer: a phase 1-2 study. Lancet. 2010; 375:1437–46. [PubMed: 20398925]
9. Kinkade CW, Castillo-Martin M, Puzio-Kuter A, Yan J, Foster TH, Gao H, et al. Targeting AKT/mTOR and ERK MAPK signaling inhibits hormone-refractory prostate cancer in a preclinical mouse model. J Clin Invest. 2008; 118:3051–64. [PubMed: 18725989]
10. Kremer CL, Klein RR, Mendelson J, Browne W, Samadzedeh LK, Vanpatten K, et al. Expression of mTOR signaling pathway markers in prostate cancer progression. Prostate. 2006; 66:1203–12. [PubMed: 16652388]
11. Rivera VM, Squillace RM, Miller D, Berk L, Wardwell SD, Ning Y, et al. Ridaforolimus (AP23573; MK-8669), a potent mTOR inhibitor, has broad antitumor activity and can be optimally administered using intermittent dosing regimens. Molecular cancer therapeutics. 2011; 10:1059–71. [PubMed: 21482695]
12. Taylor BS, Schultz N, Hieronymus H, Gopalan A, Xiao Y, Carver BS, et al. Integrative genomic profiling of human prostate cancer. Cancer Cell. 2010; 18:11–22. [PubMed: 20579941]
13. Gao H, Ouyang X, Banach-Petrosky WA, Shen MM, Abate-Shen C. Emergence of androgen independence at early stages of prostate cancer progression in Nkx3.1; Pten mice. Cancer Res. 2006; 66:7929–33. [PubMed: 16912166]
14. Uzgare AR, Isaacs JT. Enhanced redundancy in Akt and mitogen-activated protein kinase-induced survival of malignant versus normal prostate epithelial cells. Cancer Res. 2004; 64:6190–9. [PubMed: 15342404]
15. Dancey J. mTOR signaling and drug development in cancer. Nat Rev Clin Oncol. 2010; 7:209–19. [PubMed: 20234352]
16. Sawyers CL. Will mTOR inhibitors make it as cancer drugs? Cancer Cell. 2003; 4:343–8. [PubMed: 14667501]
17. Yap TA, Yan L, Patnaik A, Fearen I, Olmos D, Papadopoulos K, et al. First-in-Man Clinical Trial of the Oral Pan-AKT Inhibitor MK-2206 in Patients With Advanced Solid Tumors. J Clin Oncol. 2011
18. Carracedo A, Ma L, Teruya-Feldstein J, Rojo F, Salmena L, Alimonti A, et al. Inhibition of mTORC1 leads to MAPK pathway activation through a PI3K-dependent feedback loop in human cancer. J Clin Invest. 2008; 118:3065–74. [PubMed: 18725988]
19. Choo AY, Yoon SO, Kim SG, Roux PP, Blenis J. Rapamycin differentially inhibits S6Ks and 4E-BP1 to mediate cell-type-specific repression of mRNA translation. Proc Natl Acad Sci U S A. 2008; 105:17414–9. [PubMed: 18955708]
20. Wan X, Harkavy B, Shen N, Grohar P, Helman LJ. Rapamycin induces feedback activation of Akt signaling through an IGF-1R-dependent mechanism. Oncogene. 2007; 26:1932–40. [PubMed: 17001314]
21. Breuleux M, Klopfenstein M, Stephan C, Doughty CA, Barys L, Maira SM, et al. Increased AKT S473 phosphorylation after mTORC1 inhibition is rictor dependent and does not predict tumor cell response to PI3K/mTOR inhibition. Mol Cancer Ther. 2009; 8:742–53. [PubMed: 19372546]
22. Sharma A, Yeow WS, Ertel A, Coleman I, Clegg N, Thangavel C, et al. The retinoblastoma tumor suppressor controls androgen signaling and human prostate cancer progression. J Clin Invest. 2010; 120:4478–92. [PubMed: 21099110]
23. Sharma A, Comstock CE, Knudsen ES, Cao KH, Hess-Wilson JK, Morey LM, et al. Retinoblastoma tumor suppressor status is a critical determinant of therapeutic response in prostate cancer cells. Cancer Res. 2007; 67:6192–203. [PubMed: 17616676]
24. Wang X, Kruithof-de Julio M, Economides KD, Walker D, Yu H, Halili MV, et al. A luminal epithelial stem cell that is a cell of origin for prostate cancer. Nature. 2009; 461:495–500. [PubMed: 19741607]

NIH-PA Author Manuscript

NIH-PA Author Manuscript

NIH-PA Author Manuscript

25. Lesche R, Groszer M, Gao J, Wang Y, Messing A, Sun H, et al. Cre/loxP-mediated inactivation of the murine Pten tumor suppressor gene. Genesis. 2002; 32:148–9. [PubMed: 11857804]
26. Bhatia-Gaur R, Donjacour AA, Sciavolino PJ, Kim M, Desai N, Young P, et al. Roles for Nkx3.1 in prostate development and cancer. Genes Dev. 1999; 13:966–77. [PubMed: 10215624]
27. Chen Z, Trotman LC, Shaffer D, Lin HK, Dotan ZA, Niki M, et al. Crucial role of p53-dependent cellular senescence in suppression of Pten-deficient tumorigenesis. Nature. 2005; 436:725–30. [PubMed: 16079851]
28. Subramanian A, Tamayo P, Mootha VK, Mukherjee S, Ebert BL, Gillette MA, et al. Gene set enrichment analysis: a knowledge-based approach for interpreting genome-wide expression profiles. Proc Natl Acad Sci U S A. 2005; 102:15545–50. [PubMed: 16199517]
29. Croft D, O'Kelly G, Wu G, Haw R, Gillespie M, Matthews L, et al. Reactome: a database of reactions, pathways and biological processes. Nucleic Acids Res. 2011; 39:D691–7. [PubMed: 21067998]
30. Ogata H, Goto S, Sato K, Fujibuchi W, Bono H, Kanehisa M. KEGG: Kyoto Encyclopedia of Genes and Genomes. Nucleic Acids Res. 1999; 27:29–34. [PubMed: 9847135]
31. Abate-Shen C, Shen MM, Gelmann E. Integrating differentiation and cancer: the Nkx3.1 homeobox gene in prostate organogenesis and carcinogenesis. Differentiation. 2008; 76:717–27. [PubMed: 18557759]
32. Carracedo A, Alimonti A, Pandolfi PP. PTEN level in tumor suppression: how much is too little? Cancer Res. 2011; 71:629–33. [PubMed: 21266353]
33. Nardella C, Carracedo A, Salmena L, Pandolfi PP. Faithfull modeling of PTEN loss driven diseases in the mouse. Curr Top Microbiol Immunol. 2010; 347:135–68. [PubMed: 20549475]
34. Abate-Shen C, Banach-Petrosky WA, Sun X, Economides KD, Desai N, Gregg JP, et al. Nkx3.1; Pten mutant mice develop invasive prostate adenocarcinoma and lymph node metastases. Cancer Res. 2003; 63:3886–90. [PubMed: 12873978]
35. Kim MJ, Cardiff RD, Desai N, Banach-Petrosky WA, Parsons R, Shen MM, et al. Cooperativity of Nkx3.1 and Pten loss of function in a mouse model of prostate carcinogenesis. Proc Natl Acad Sci U S A. 2002; 99:2884–9. [PubMed: 11854455]
36. Carver BS, Chapinski C, Wongvipat J, Hieronymus H, Chen Y, Chandarlapaty S, et al. Reciprocal feedback regulation of PI3K and androgen receptor signaling in PTEN-deficient prostate cancer. Cancer Cell. 2011; 19:575–86. [PubMed: 21575859]
37. Trotman LC, Niki M, Dotan ZA, Koutcher JA, Di Cristofano A, Xiao A, et al. Pten dose dictates cancer progression in the prostate. PLoS Biol. 2003; 1:E59. [PubMed: 14691534]
38. Wang S, Gao J, Lei Q, Rozengurt N, Pritchard C, Jiao J, et al. Prostate-specific deletion of the murine Pten tumor suppressor gene leads to metastatic prostate cancer. Cancer Cell. 2003; 4:209–21. [PubMed: 14522255]
39. Mulholland DJ, Tran LM, Li Y, Cai H, Morim A, Wang S, et al. Cell autonomous role of PTEN in regulating castration-resistant prostate cancer growth. Cancer Cell. 2011; 19:792–804. [PubMed: 21620777]
40. Shen MM, Abate-Shen C. Pten inactivation and the emergence of androgen-independent prostate cancer. Cancer Res. 2007; 67:6535–8. [PubMed: 17638861]
41. Wu X, Wu J, Huang J, Powell WC, Zhang J, Matusik RJ, et al. Generation of a prostate epithelial cell-specific Cre transgenic mouse model for tissue-specific gene ablation. Mech Dev. 2001; 101:61–9. [PubMed: 11231059]
42. Park JH, Walls JE, Galvez JJ, Kim M, Abate-Shen C, Shen MM, et al. Prostatic intraepithelial neoplasia in genetically engineered mice. Am J Pathol. 2002; 161:727–35. [PubMed: 12163397]
43. Mazzoletti M, Bortolin F, Brunelli L, Pastorelli R, Di Giandomenico S, Erba E, et al. Combination of PI3K/mTOR inhibitors: antitumor activity and molecular correlates. Cancer Res. 2011; 71:4573–84. [PubMed: 21602434]
44. Cheng Y, Zhang Y, Zhang L, Ren X, Huber-Keener KJ, Liu X, et al. MK-2206, a novel allosteric inhibitor of Akt, synergizes with gefitinib against malignant glioma via modulating both autophagy and apoptosis. Mol Cancer Ther. 2011
45. Hirai H, Sootome H, Nakatsuru Y, Miyama K, Taguchi S, Tsujioka K, et al. MK-2206, an allosteric Akt inhibitor, enhances antitumor efficacy by standard chemotherapeutic agents or

NIH-PA Author Manuscript

NIH-PA Author Manuscript

NIH-PA Author Manuscript

molecular targeted drugs in vitro and in vivo. Mol Cancer Ther. 2010; 9:1956–67. [PubMed: 20571069]

46. Hartford CM, Desai AA, Janisch L, Karrison T, Rivera VM, Berk L, et al. A phase I trial to determine the safety, tolerability, and maximum tolerated dose of deforolimus in patients with advanced malignancies. Clin Cancer Res. 2009; 15:1428–34. [PubMed: 19228743]
47. Rizzieri DA, Feldman E, Dipersio JF, Gabrail N, Stock W, Strair R, et al. A phase 2 clinical trial of deforolimus (AP23573, MK-8669), a novel mammalian target of rapamycin inhibitor, in patients with relapsed or refractory hematologic malignancies. Clin Cancer Res. 2008; 14:2756–62. [PubMed: 18451242]
48. Mita MM, Mita AC, Chu QS, Rowinsky EK, Fetterly GJ, Goldston M, et al. Phase I trial of the novel mammalian target of rapamycin inhibitor deforolimus (AP23573; MK-8669) administered intravenously daily for 5 days every 2 weeks to patients with advanced malignancies. J Clin Oncol. 2008; 26:361–7. [PubMed: 18202410]
49. Sobel RE, Sadar MD. Cell lines used in prostate cancer research: a compendium of old and new lines--part 1. J Urol. 2005; 173:342–59. [PubMed: 15643172]
50. Phung TL, Ziv K, Dabydeen D, Eyiah-Mensah G, Riveros M, Perruzzi C, et al. Pathological angiogenesis is induced by sustained Akt signaling and inhibited by rapamycin. Cancer Cell. 2006; 10:159–70. [PubMed: 16904613]
51. Chen HZ, Tsai SY, Leone G. Emerging roles of E2Fs in cancer: an exit from cell cycle control. Nat Rev Cancer. 2009; 9:785–97. [PubMed: 19851314]
52. Guertin DA, Stevens DM, Saitoh M, Kinkel S, Crosby K, Sheen JH, et al. mTOR complex 2 is required for the development of prostate cancer induced by Pten loss in mice. Cancer Cell. 2009; 15:148–59. [PubMed: 19185849]
53. Lamming DW, Ye L, Katajisto P, Goncalves MD, Saitoh M, Stevens DM, et al. Rapamycin-induced insulin resistance is mediated by mTORC2 loss and uncoupled from longevity. Science. 2012; 335:1638–43. [PubMed: 22461615]
54. Nardella C, Clohessy JG, Alimonti A, Pandolfi PP. Pro-senescence therapy for cancer treatment. Nat Rev Cancer. 2011; 11:503–11. [PubMed: 21701512]

NIH-PA Author Manuscript
NIH-PA Author Manuscript
NIH-PA Author Manuscript

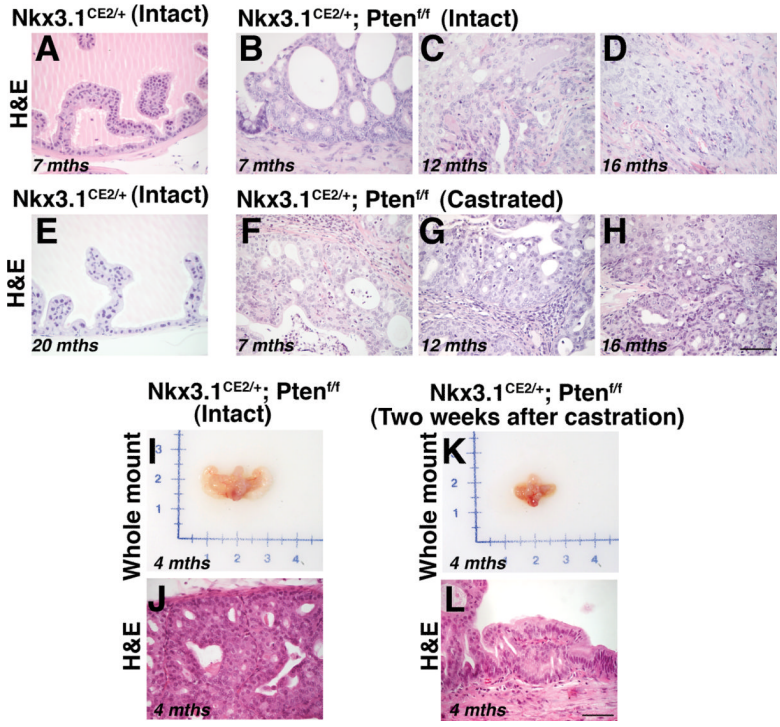

Figure 1. Histological analyses of intact and castrated mouse prostate phenotypes

(A-H) Phenotype of castrated and intact prostate. H&E of anterior prostate from intact or castrated *Nkx3.1*$^{CE2/+}$ or *Nkx3.1*$^{CE2/+}$*; Pten*$^{f/f}$ mice. Mice at two months of age were induced with tamoxifen to form tumors; the ages indicated refer to the time following tumor induction. (I-L) Analyses of tumor regression following castration. Mice were induced to form tumors at 2 months of age (as above) and then castrated (or left intact) 4 months later. Shown are whole mount images of the urogenital regions including prostate *(I, K)*, or H&E two weeks after castration (or mock surgery) *(J, L)*.

Scale bars represent 100 mm.

NIH-PA Author Manuscript
NIH-PA Author Manuscript
NIH-PA Author Manuscript

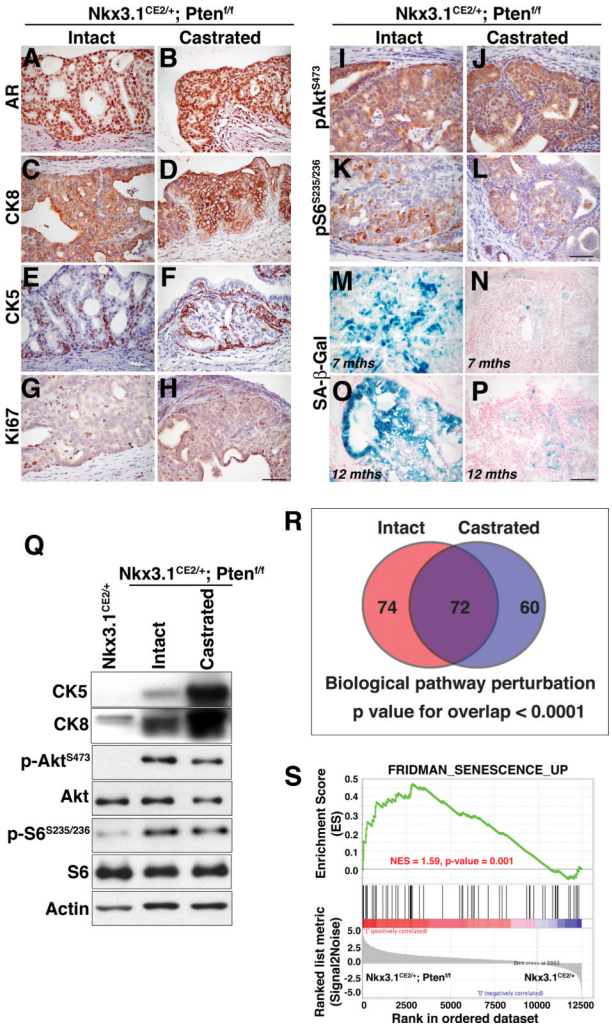

Figure 2. Phenotypic analyses of the prostate phenotype from intact versus castrated *Nkx3.1*$^{CE2/+}$;*Pten*$^{f/f}$ mice

(A-P) Marker analyses of anterior prostate. Mice were induced with tamoxifen to form tumors at two months of age, castrated or left intact at 4 months later, and then analyzed 12 months following tumor induction (unless otherwise indicated). (A, B) Immunostaining for androgen receptor (AR) shows similar levels of nuclear AR in intact and castrated mice. (C-D) Immunostaining for cytokeratin 8 (CK8) shows the predominance of luminal cells in the prostate of both intact and castrated mice. (C-F) Immunostaining for cytokeratin 5 (CK5), shows enrichment of basal cells in the prostate of castrated mice. (G, H) Immunostaining for Ki67 shows high level of proliferative activity in the prostates of both intact and castrated mice. (I-L) Immunostaining for p-Akt^{Ser473} and for p-S6$^{S235/236}$ indicate strong activation of Akt and mTOR signaling both in the intact and castrated mice. (M, P) SA-β-gal staining shows robust expression in the intact but not castrated prostate both at 7 or 12 months following tumor induction. (Q) Western blot analyses using total protein extracts from dorsal prostate of mice from the indicated genotypes, 12 months following tumor induction. (R, S) Analyses of differential gene expression analyses from intact versus castrated *Nkx3.1*$^{CE2/+}$ or *Nkx3.1*$^{CE2/+}$; *Pten*$^{f/f}$ mice (see Supplementary Tables 3, 4). (R) Venn diagram summarizing the overlap in biological pathways, identified using GSEA (see Supplementary Table 5, 6), which are differentially expressed in intact or castrated *Nkx3.1*$^{CE2/+}$; *Pten*$^{f/f}$ prostate. (S) GSEA analyses shows enrichment of a senescence

NIH-PA Author Manuscript

NIH-PA Author Manuscript

NIH-PA Author Manuscript

signature in the intact *Nkx3.1*$^{CE2/+}$; *Pten*$^{f/f}$ mouse prostate tumor. Shown on the x-axis is the rank-order of mouse genes from the most up-regulated (position 1) to the most down-regulated (position 12,435) between the intact *Nkx3.1*$^{CreERT2/+}$; *Pten*$^{f/f}$ versus the control *Nkx3.1*$^{CreERT2/+}$ mice; the barcode indicates the position of genes from the indicated human biological pathway. The y-axis corresponds to the running enrichment score (ES) generated by the cumulative tally of the pathway genes. The total height of the curve indicates the extent of enrichment, with the normalized enrichment score (NES) and p-values indicated. Scale bars represent 100 mm.

NIH-PA Author Manuscript

NIH-PA Author Manuscript

NIH-PA Author Manuscript

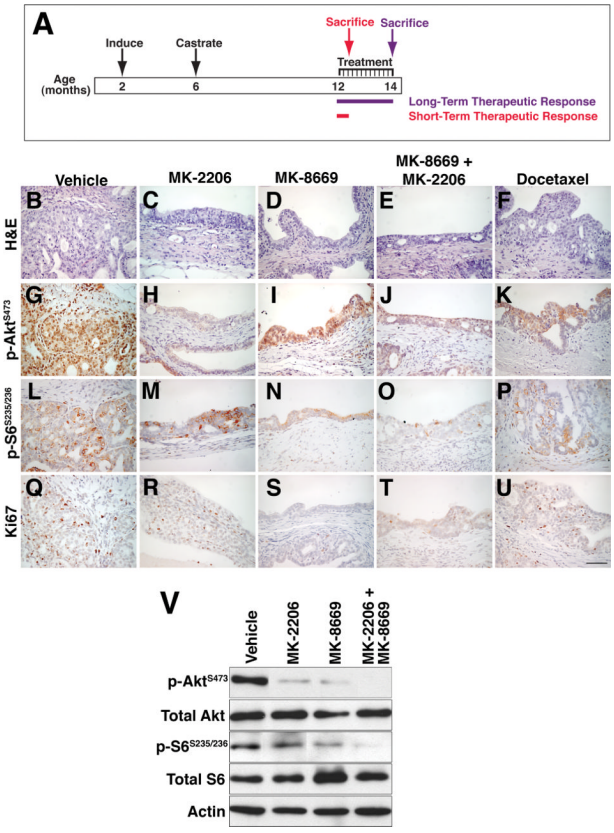

Figure 3. Dual targeting Akt/mTOR signaling inhibits castration resistant prostate cancer

(A) Design of preclinical studies to evaluate combination treatment with MK-2206 and MK-8669 for castration-resistant prostate cancer. *Nkx3.1*$^{CreERT2/+}$; *Pten*$^{f/f}$ mice were induced with tamoxifen at 2 months of age and castrated 4 months later (at 6 months). Treatment (with MK-2206 and/or MK-8669 or docetaxel) was initiated 10 months after tamoxifen induction (at 12 months) and continued for 2 months following which mice were sacrificed for analyses. (B-F) Representative H&E images showing the histology of the anterior prostate of mice treated with agents as indicated. (G-P) Immunostaining for p-Akt and p-S6 showing reduced immunostaining following treatment with their respective inhibitors, MK-2206 and MK-8669, as was also evident by Western blotting (see Panel V). (Q-U) Analyses of cellular proliferation by immunostaining for Ki67; quantitation of the data is shown in Table 2. (V) Western blot analyses of tissues from the short-term treated mice showing relative expression of Akt/mTOR pathway markers following drug treatment. Scale bars represent 100 mm.

NIH-PA Author Manuscript
NIH-PA Author Manuscript
NIH-PA Author Manuscript

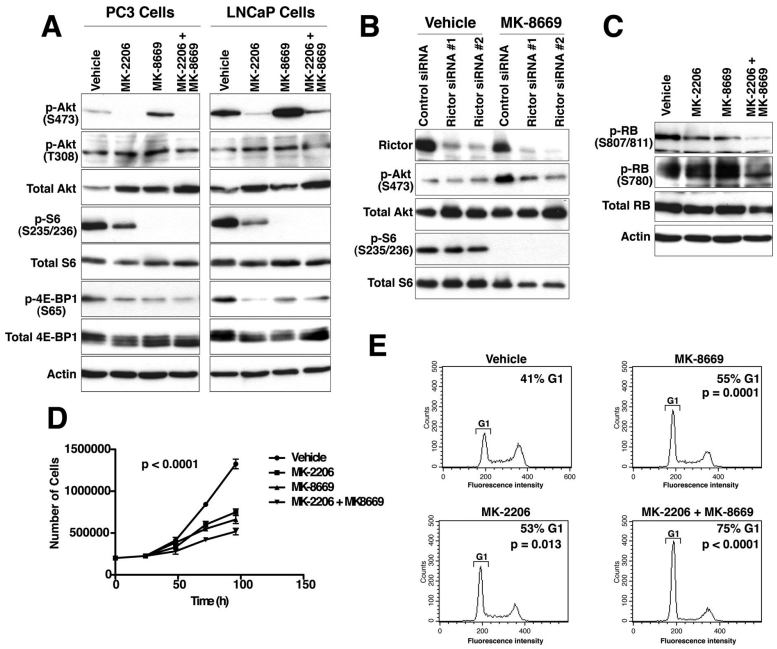

Figure 4. Analyses of MK-2206 and MK-8669 on human prostate cancer cells

(A) Western blot analyses of protein extracts from PC3 or LNCaP cells, as indicated, showing the expression levels of the indicated phospho-proteins following treatment with agents, as indicated, for 24 hours. (B) Western blot analyses of PC3 cells incubated with the control or Rictor siRNA for 24 hours, followed by treatment with the agents as indicated for an additional 24 hours. (C) Western blot analyses of PC3 cells showing the expression levels of the indicated phospho-proteins following treatment with the agents, as indicated, for 24 hours. (D) Cell growth assay. PC3 cells were seeded at low density (200,000/35 mm dish) on day 0 and then treated on day 1 with vehicle or MK-2206 (1 μM) and/or MK-8669 (1 nM). Cell numbers were assessed by counting with trypan blue. (E) Flow cytometry analyses of PC3 cells showing the percentage of cells in the G1 phase following treatment with the indicated drug for 24 hours; similar results were obtained following incubation for 48 hours.

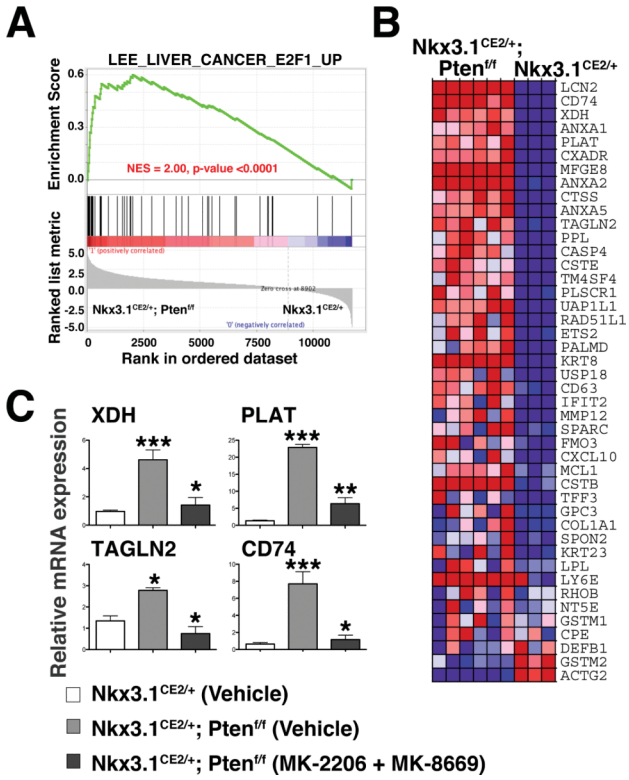

Figure 5. Analyses of E2F1 pathway expression in mouse prostate cancer cells

(A) GSEA analyses showing enrichment of an E2F signature in the castrated *Nkx3.1*$^{CE2/+}$; *Pten*$^{f/f}$ mice. Shown on the x-axis is the rank-order of mouse genes from the most up-regulated (position 1) to the most down-regulated (position 11,726) between the castrated *Nkx3.1*$^{CreERT2/+}$; *Pten*$^{f/f}$ versus the control (intact) *Nkx3.1*$^{CreERT2/+}$ mice; the barcode indicates the position of genes from the indicated human biological pathway. The y-axis corresponds to the running enrichment score (ES) generated by the cumulative tally of the pathway genes. The total height of the curve indicates the extent of enrichment, with the normalized enrichment score (NES) and p-values indicated. (B) Heat map of leading edge genes. (C) Real-time PCR validation of selected genes. Note that the *Nkx3.1*$^{CreERT2/+}$ mice are intact, while the *Nkx3.1*$^{CreERT2/+}$; *Pten*$^{f/f}$ with vehicle or drug treatment are castrated.

NIH-PA Author Manuscript NIH-PA Author Manuscript NIH-PA Author Manuscript

NIH-PA Author Manuscript NIH-PA Author Manuscript NIH-PA Author Manuscript

Table 1

Summary of prostate cancer phenotype

Group	Genotype	N	Age	Pathological description	% Ki67 cells
Control	Nkx3.1$^{CreERT2/+;}$ Pten$^{+/+}$	6	8	Hyperplasia, low-grade PIN (similar to *Nkx3.1* phenotype)	3%
Intact	Nkx3.1$^{CreERT2/+;}$ Pten$^{flox/flox}$	10	6-9	PIN I, PIN II, and PIN III	ND
		8	9-12	Extensive PIN III and PIN IV, with some (2 out of 8 mice) having areas of squamous carcinoma	12%
		8	16+	Extensive PIN III and PIN IV, with some (2 out of 8 mice) having areas of solitary or extensive squamous metaplasia; acute inflammation and submucosal proliferation of Pale cells.	ND
Castrated	Nkx3.1$^{CreERT2/+;}$ Pten$^{flox/flox}$	12	6-9	PIN I, PIN II and PIN III	ND
		14	9-12	PIN II, PIN III and PIN IV with extensive fibrosis and inflammation; some (3 out of 14 mice) having areas of solitary or extensive squamous metaplasia	14%
		14	16+	Microinvasive adenocarcinoma with areas of poorly differentiated adenocarcinoma; some mice (2 out of 14 mice) having areas of large fibrous nodules lined by a glandular epithelium with extensive squamous metaplasia	ND

Legend: Summary of the prostate cancer phenotype of the mouse models used in this study. The numbers of mice analyzed are indicated; the age refers to the time following tumor induction. The pathological description follows the pathological classification of Park et al. (42). The % Ki67 staining refers to the total number of Ki67 positive epithelial cells relative to the total number of epithelial cells. N, refers to the total number of mice analyzed; ND, not determined.

Cancer Res. Author manuscript; available in PMC 2013 September 01.

NIH-PA Author Manuscript

NIH-PA Author Manuscript

NIH-PA Author Manuscript

Table 2

Summary of Tumor weights and proliferation of prostate tumor from castrated *Nkx3.1*$^{CE2/+}$;*Pten*$^{f/f}$ mice.

Treatment	N	Weight (grams)	Proliferation
Vehicle	6	0.38 ± 0.01	11% ± 1.1
MK-2206	6	0.23 ± 0.06 $p = 0.27$	15% ± 3.1 $p = 0.20$
MK-8669	6	0.34 ± 0.22 $p = 0.90$	3% ± 0.7 $p < 0.001$
MK-2206+MK-8669	7	0.03 ± 0.005 $p = 0.004$	4% ± 1.0 $p < 0.001$
Docetaxel	4	0.19 ± 0.05 $p = 0.080$	17% ± 1.6 $p = 0.005$

Legend: Summary of the data for castrated *Nkx3.1*$^{CE2/+}$;*Pten*$^{f/f}$ mice showing the average tumor weights and percentage of proliferating epithelial cells following the indicated treatment. Where indicated, *p*-values compare the drug-treated to vehicle-treated groups N, refers to the total number of mice analyzed